Torque-Fill Control and Energy Management for a Four-Wheel-Drive Electric Vehicle Layout With Two-Speed Transmissions

Stefano De Pinto, Pablo Camocardi, Aldo Sorniotti, *Member, IEEE*, Patrick Gruber, Pietro Perlo, and Fabio Viotto

Abstract—This paper presents a novel four-wheel-drive electric vehicle layout consisting of one on-board electric drivetrain per axle. Each drivetrain includes a simplified clutch-less two-speed transmission system and an open differential to transmit the torque to the wheels. This drivetrain layout allows eight different gear state combinations at the vehicle level, thus increasing the possibility of running the vehicle in a more energy-efficient state for the specific wheel torque demand and speed. To compensate for the torque gap during gearshifts, a "torque-fill" controller was developed that varies the motor torque on the axle not involved in the gearshift. Experimental tests show the effectiveness of the developed gearshift strategy extended with the torque-fill capability. Energy efficiency benefits are discussed by comparing the energy consumptions of the case study vehicle controlled through a constant front-to-total wheel torque distribution and conventional gearshift maps, and the same vehicle with an energy management system based on an offline optimization. Results demonstrate that the more advanced controller brings a significant reduction of the energy consumption at constant speed and along different driving cycles.

Index Terms—Electric vehicle (EV), four-wheel-drive (4WD), state selection, torque distribution, torque-fill, two-speed transmission.

NOMENCLATURE

a	Longitudinal acceleration.
APP	Accelerator pedal position.
AR	Gearshift performance indicator related to the area ratio of the desired and actual longitudinal acceleration profiles during a gearshift.
F	Force.
g	Gravity.
h	Index indicating the vehicle speed value within the discretized grid (also used as a subscript).
i	Transmission gear ratio.
l	Index indicating the front-to-total wheel torque distribution.
IAE	Gearshift performance indicator related to the integral of the absolute value of the longitudinal acceleration error.
j	Index indicating the wheel torque value (also used as a subscript).
J	Mass moment of inertia.
k	Torsional stiffness.
m	Mass.
n	Index indicating the vehicle state number.
P	Power.
PTPA	Gearshift performance indicator related to the peak-to-peak difference within the longitudinal acceleration profile during a gearshift.
R	Radius.
s	Laplace operator.
t	Time.
T	Torque.
V	Vehicle speed.
x	Gear actuator position.
y	Nondimensional factor for the computation of the reference motor speed during gearshifts.
α	Angle describing the longitudinal road gradient.
β	Torsional damping coefficient.
η	Efficiency.
$\theta, \dot{\theta}, \ddot{\theta}$	Angular position, speed, acceleration.
τ	Time constant or pure time delay.

The following superscripts and subscripts are used in the paper:

act	Gearbox actuator.
Aero	Aerodynamic drag.
app	Apparent.
d	Delay.
desired	Desired (or reference) value.
diff	Differential.
dis	Disengaged.
EM	Electric motor.
EMS	Energy management system.
EM + D	Electric motor and drive.

S. De Pinto, A. Sorniotti, and P. Gruber are with the Department of Mechanical Engineering Sciences, University of Surrey, Guildford GU2 7XH, U.K. (e-mail: s.depinto@surrey.ac.uk; a.sorniotti@surrey.ac.uk; p.gruber@surrey.ac.uk).

P. Camocardi was with the University of Surrey, Guildford GU2 7XH, U.K. He is now with Advanced Development, Brose Fahrzeugteile GmbH and Company, 97076 Würzburg, Germany (e-mail: pablo.camocardi@brose.com).

P. Perlo is with Interactive Fully Electric Vehicles, 10098 Turin, Italy (e-mail: pietro.perlo@ifevs.com).

F. Viotto is with EV & HV Transmissions Automotive Applications, Oerlikon Graziano SpA, 10098 Turin, Italy (e-mail: fabio.viotto@oerlikon.com).

eq	Equivalent.
f	Front.
filt	Filter.
$g1$, $g2$, dis	Gear 1, gear 2, disengaged gear.
HS	Half-shaft.
in, fin	Initial, final.
IP	Inertia phase.
l	Index indicating the front-to-total wheel torque distribution.
L	Left.
Loss	Loss (referred to a power).
MAX	Maximum possible value of a variable.
n	Index indicating the vehicle state number.
PS, SS	Primary shaft, secondary shaft.
r	Rear.
R	Right.
Roll	Rolling resistance.
sel	Selected gear ratio (first, second, or neutral).
TF	Torque-fill enabled.
TCU	Transmission control unit.
Tr	Transmission.
w	Wheel.
$w\&f$	Windage and friction.
$*$	Optimal value.

Fig. 1. Example of the overall efficiency map of an electric drivetrain equipped with (a) single-speed and (b) two-speed transmission systems.

I. INTRODUCTION

ELECTRIC vehicles (EVs) are usually characterized by the on-board installation of a single electric drivetrain, consisting of an electric motor (EM) with its inverter, a single-speed transmission, an open differential, constant velocity joints, and half-shafts [1] [2]. In this context, multiple-speed transmissions for EVs are a growing area of research, as they open up new development avenues for drivetrain configurations [3].

The need for multiple-speed transmissions arises from the typical characteristics of EMs, providing maximum torque at low speeds. At higher speeds, their operation is usually limited to an approximately constant power region, sometimes followed by a region with decreasing power as a function of speed [1], [2]. Especially in the case of EMs with a limited speed range, single-speed transmissions have to be designed as a tradeoff between gradeability (which requires a high gear ratio) and top speed (which requires a low gear ratio [4]). For this reason, the top speed of EVs with a single-speed transmission is often limited by the maximum speed of the motor rather than its power. In contrast, a two-speed electric drivetrain allows the first gear ratio to provide the desired longitudinal acceleration and gradeability performance, while the second gear can be selected to reach a specified top speed. As a result, two-speed electric drivetrains extend the available wheel torque characteristic as a function of vehicle speed. Fig. 1(a) and (b) reports the boundaries of the wheel torque characteristics, respectively for single-speed and two-speed electric drivetrains with the same motor, for an axle of the EV demonstrator of this research.

In addition, as the efficiency of an electric drivetrain is a function of torque and speed, a two-speed transmission system allows increased flexibility in the selection of the operating point for assigned vehi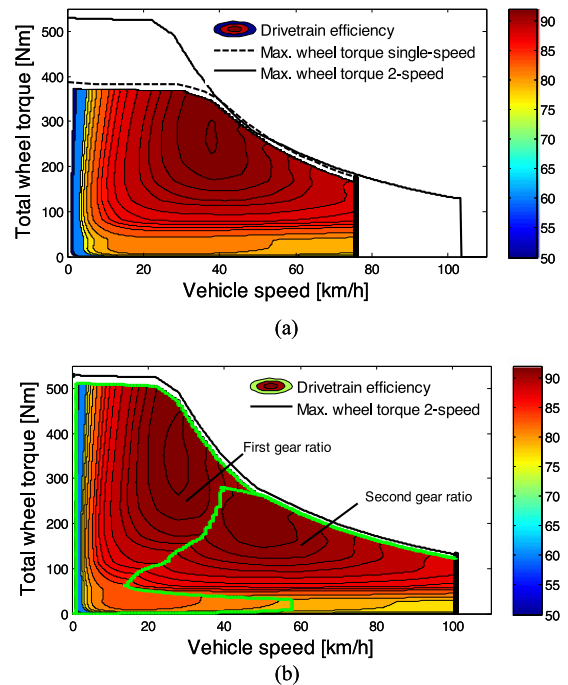cle speed and wheel torque demand, thus bringing potential energy efficiency benefits [5]. For example, Fig. 1(a) shows the combined efficiency values of the EM drive and single-speed transmission for an axle of the case study vehicle. The region of maximum efficiency ($\sim$93%) of the electric drivetrain is for medium values of torque and speed, e.g., approximately at 40 km/h and 270 N·m in Fig. 1(a). The adoption of a two-speed transmission [see Fig. 1(b)] extends the region of high efficiency to speeds from 20 to 60 km/h. The borders of the regions corresponding to the first and second gear ratios are shown in the figure by the green line. In Fig. 1(b), the gear selection was computed offline to provide maximum overall drivetrain efficiency. In the offline calculations, transmission efficiency has to be included in the form of a map (e.g., as a function of the selected gear, torque, speed, and temperature), as in modern electric drivetrains the values of transmission efficiency are of similar order of magnitude to those of EM drives.

Despite the potential benefits, the main barrier for the adoption of multiple-speed transmissions in EVs is the increase in system complexity, cost, and mass. In terms of complexity, the gearshift process requires a sequence of mechanical steps, which can be difficult to control [6]–[11]. In particular, one of the main potential drawbacks of multiple-speed transmissions is the disruption of the wheel torque during gearshifts, i.e., the torque gap, which increases acceleration times and impairs ride comfort. To avoid torque gaps, seamless gearshift methodologies were developed, based on complex transmission layouts, such as dual-clutch transmissions [12], continuously variable transmissions [13], and novel dual-motor drivetrains [3].

In parallel, the actual achievement of the potential energy efficiency enhancement associated with the adoption of multiple-speed transmissions and four-wheel-drive (4WD) EV architectures requires complex controllers for the selection of

Fig. 2. Case study vehicle prototype.

the optimal state and front-to-total wheel torque distribution. These algorithms are often based on advanced control structures (for example, discussed in [14]–[16]), with potentially difficult industrial implementation. Moreover, the outputs of the energy-efficiency-oriented control systems can be unacceptable, in practice, in terms of vehicle drivability. Finally, to the knowledge of the authors of this paper, the energy-efficient controllers in the literature are focused on two-wheel-drive EVs with multiple-speed transmissions and on 4WD EVs with single-speed transmissions or in-wheel configurations. These EV setups are simpler to control during straight-line operation than the EV configuration of this study, combining the flexibility offered by the 4WD architecture and the two-speed transmissions.

With respect to the previous points, the main contributions of the paper are the following.

1) The analysis of a novel 4WD EV architecture including mechanically simple two-speed transmission systems, without clutches or synchronizers.
2) The implementation and experimental validation of a torque-fill controller based on the torque control of the drivetrain not involved in the gearshift, in order to compensate for the torque gap caused by the other drivetrain.
3) The discussion of a computationally efficient energy management system (EMS) for the selection of the optimal gear ratios and front-to-total wheel torque distribution.

This paper is organized as follows. Section II introduces the EV architecture proposed by the European Union funded projects PLUS-MOBY and FREE-MOBY [17]. The corresponding vehicle simulation model is explained in Section III. Section IV describes the torque-fill control function during gearshifts, which is the precondition for the actual implementation of effective state-selection algorithms. Section V presents the optimization algorithm used to derive the optimal gear state and front-to-total wheel torque distribution. Section VI shows the experimental results with the proposed gearshift strategy, and the simulation results of the EMS. Finally, the main conclusions are reported in Section VII.

II. 4WD EV Configuration

The prototype vehicle of this study is an electric urban 4WD passenger car with a total mass of 730 kg (see Fig. 2), developed during the projects PLUS-MOBY and FREE-MOBY. Each axle is powered by a 14 kW (peak power) induction motor, coupled with a two-speed transmission system (see Fig. 3). The first and second gear ratios for both axles are 12.1 and 6.7, respectively [18].

The gearbox is a significant simplification of the design analyzed in [6]. In fact, the transmission does not include fric-
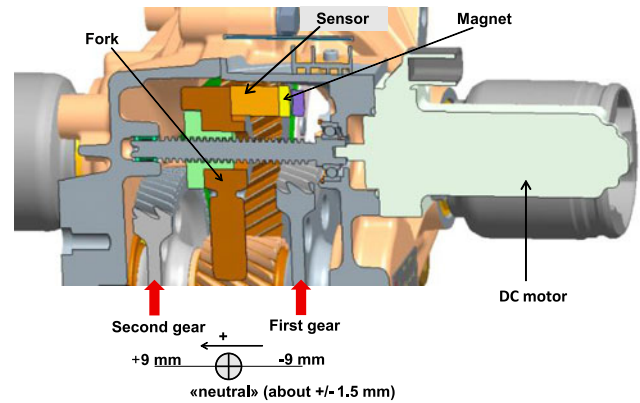

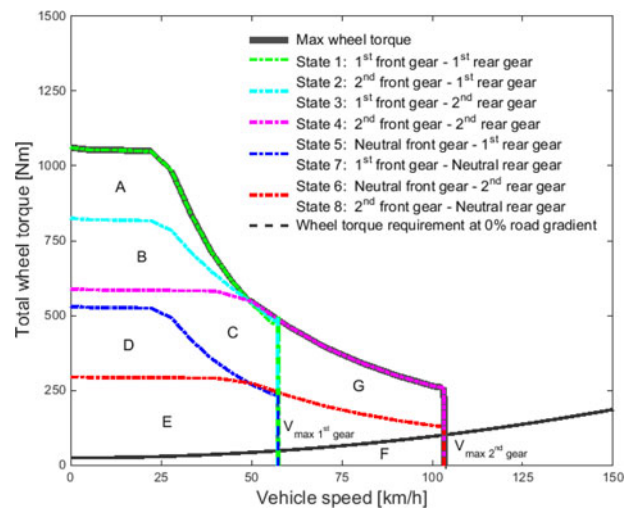Fig. 3. Cross-sectional view of the two-speed transmission prototype.

Fig. 4. Theoretical wheel torque characteristics for the eight vehicle states.

tion clutches or synchronizers, as the synchronization is carried out electrically by controlling the EM speed. The design also allows removing the friction clutch actuator, thus obtaining a mass only marginally higher than the one of the corresponding single-speed drivetrain (see also [19]). Differently from conventional step gear transmissions, the electric traction motor is never decoupled from the primary shaft of the transmission. The gears are engaged to the primary shaft through dog clutches. To shift a gear, the assembly including the selector fork and the dog clutch is actuated via a devoted DC motor, while a sensor detects the position of the actuation system (see Fig. 3). Based on the dog clutch position, three different operating conditions are possible [7]. With respect to the neutral gear reference position of 0 mm, a dog clutch position of -9 mm engages the first gear, and a position of $+9$ mm engages the second gear.

By combining the three possible states for each axle, eight state combinations are available for the case study 4WD EV layout with two-speed drivetrains (without considering the state of neutral gear on both axles). Hence, for given values of vehicle speed and wheel torque demand (correlated with the accelerator pedal position, APP), multiple states are usually possible, each of them providing a different level of energy efficiency.

More specifically, Fig. 4 shows the theoretical maximum wheel torque characteristics in traction, $T_{w,\mathrm{MAX},n}(V)$, for each

TABLE I
NUMBER OF AVAILABLE STATES FOR EACH OF THE REGIONS
(FROM A TO G) IN FIG. 4

Region	Number of states	Region	Number of states
A	1	E	8
B	3	F	3
C	4	G	1
D	6	-	-

of the vehicle states, with the obvious exclusion of the state in which both drivetrains are in neutral gear. Transmission efficiency is neglected in this preliminary simplified calculation. The different gearbox states identify seven regions (from A to G in Fig. 4 and Table I), with boundaries defined by: 1) the $T_{w,\text{MAX},n}(V)$ characteristics; and 2) the top speeds achievable in the first gear and second gear. The top-speed values are coincident for the front and rear axles, as their drivetrains are identical. Within each region, the EMS can choose among the same alternative vehicle states (see the column "Number of states" in Table I). For instance, for each point of region E, at low wheel torque and speed, eight states can be considered for the design of an efficient EMS. Moreover, for the states where both drivetrains are active, an infinite number of front-to-total wheel torque distributions can provide the same overall wheel torque.

Fig. 4 includes the torque required to make the vehicle travel at constant speed with 0% road gradient. The nominal drivetrain torque at the vehicle speed corresponding to the top speed of the motor in second gear is higher than the required wheel torque at that speed. Therefore, in conditions of 0% road gradient, vehicle speed is actually limited by motor speed (at a value of ∼105 km/h), even with the two-speed transmission. This does not represent an issue for the specific vehicle, given its expected prevalent usage in urban environments. In the case of high-speed EM drives, the tradeoff between single-speed and two-speed drivetrains is more subtle, as it is mainly based on the energy efficiency aspect.

The two independent axles can be used to reduce the torque gap during gearshifts especially for low-to-medium longitudinal accelerations, thus improving drivability. To do so, gearshifts need to be actuated on a single transmission at a time. For example, when the rear transmission is shifting a gear, hence disrupting torque at the respective wheels, the front drivetrain is used to compensate for the rear torque gap through a controlled variation of its torque demand. This results in potentially seamless gearshifts in most operating conditions, through very simple transmission hardware. However, when both motors are operating close to their maximum torque level, the system can only provide partial torque-fill.

III. EV MODEL

A detailed model of the longitudinal vehicle dynamics was implemented in MATLAB-Simulink, which simulates the two independently driven axles of the case study 4WD EV (see Fig. 5). The model was used to assess control system
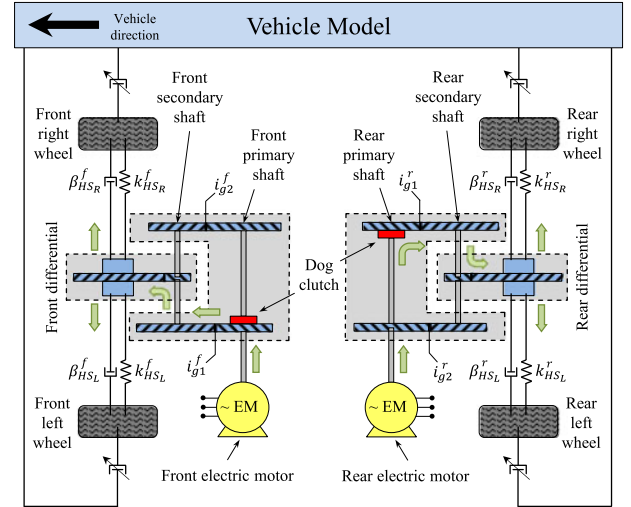

Fig. 5. Simplified layout of the 4WD vehicle model. The arrows indicate the power flow in first gear on the front and rear axles in traction conditions.

performance, alongside the experimental testing of the vehicle prototype.

The model of each axle includes the EM, gearbox, differential, half-shafts (modeled as a torsional spring and damper in parallel), and tires. The efficiency of each EM drive is simulated through the respective map as a function of torque and speed. The nonlinear tire behavior is modeled with the Pacejka Magic Formula combined with a variable relaxation length model [20].

In accordance with the possible positions of the dog clutch on each primary shaft (discussed in Section II), the transmission model simulates the three possible operating conditions of the gearbox, i.e., engaged first gear, engaged second gear, and neutral. When a gear is engaged, the approximate dynamics of the drivetrain are modeled with the equivalent inertia arising from the individual driveline components between the EM and the differential (included). Secondary effects such as plays and torsional deformations of the transmission shafts are neglected. Equations (1)–(5) are reported for the rear drivetrain. The front drivetrain model is identical to the rear one.

A. Engaged First Gear or Second Gear

In this condition, the primary and secondary shafts rotate according to the engaged gear ratio. The torque balance equation of the drivetrain in first/second gear is

$$
\ddot{\theta}_{\text{diff}}^{r} = \frac{1}{J_{\text{eq}_{g1/g2}}^{r}} \Big\{ i_{g1/g2}^{r} i_{\text{diff}}^{r} \eta_{g1/g2}^{r} T_{\text{EM}}^{r} +
$$
$$
- k_{\text{HS}_L}^{r} \left(\theta_{\text{diff}}^{r} - \theta_{w_L}^{r} \right) - \beta_{\text{HS}_L}^{r} \left(\dot{\theta}_{\text{diff}}^{r} - \dot{\theta}_{w_L}^{r} \right)
$$
$$
- k_{\text{HS}_R}^{r} \left(\theta_{\text{diff}}^{r} - \theta_{w_R}^{r} \right) - \beta_{\text{HS}_R}^{r} \left(\dot{\theta}_{\text{diff}}^{r} - \dot{\theta}_{w_R}^{r} \right) \Big\}.
$$
$$(1)$$

Within the model, transmission efficiency $\eta_{g1/g2}^{r}$ is expressed through a look-up table supplied by the manufacturer (Oerlikon Graziano SpA), which is a function of the selected gear, motor torque, primary shaft speed, and transmission temperature.

The look-up table is based on the results of a detailed steady-state model of the transmission power losses (e.g., caused by gear meshing, bearings, windage, and churning), which was experimentally validated for other transmission configurations. In (1) and in the remainder of the paper, the factor $\eta^r_{g1/g2}$ is reported for the case of traction (a factor $1/\eta^r_{g1/g2}$ should be considered during regeneration). The equivalent mass moment of inertia of the drivetrain in first/second gear is

$$
\begin{aligned}
J^r_{\mathrm{eq}_{g1/g2}} = {} & J^r_{\mathrm{diff}} + 0.5 \left(J^r_{\mathrm{HS_R}} + J^r_{\mathrm{HS_L}} \right) \\
& + \left(J^r_{\mathrm{SS}} + J^r_{g2/g1} i^r_{g2/g1}{}^2 \right) i^r_{\mathrm{diff}}{}^2 \\
& + \left(J^r_{\mathrm{EM}} + J^r_{\mathrm{PS}} + J^r_{g1/g2} \right) i^r_{g1/g2}{}^2 i^r_{\mathrm{diff}}{}^2 \eta^r_{g1/g2}.
\end{aligned}
\tag{2}
$$

The formulation corresponding to (1) and (2) is used only for the simulation of conditions with symmetric behavior of the two wheels of the same axle (i.e., symmetric half-shafts and tire-road parameters). For more complex situations (e.g., asymmetric tire–road friction conditions), a model including the dynamics of the differential internals is adopted, according to the approach described in [21].

B. Neutral

In this condition, the drivetrain model is characterized by an additional degree of freedom (DoF), as the EM dynamics are decoupled from the transmission output shaft dynamics. Hence, the first DoF relates to the rotating parts of the EM and transmission components rigidly connected to the primary shaft. The second DoF refers to the transmission's secondary shaft and the differential. In formulas

$$
\begin{cases}
\ddot{\theta}^r_{\mathrm{EM}} = \dfrac{T^r_{\mathrm{EM}} - T^r_{wf}}{J^r_{\mathrm{EM}} + J^r_{\mathrm{PS}}} \\[2mm]
\ddot{\theta}^r_{\mathrm{diff}} = \dfrac{1}{J^r_{\mathrm{eq}_{dis}}} \left\{ -k^r_{\mathrm{HS_L}} \left(\theta^r_{\mathrm{diff}} - \theta^r_{w_L} \right) - \beta^r_{\mathrm{HS_L}} \left(\dot{\theta}^r_{\mathrm{diff}} - \dot{\theta}^r_{w_L} \right) \right. \\[1mm]
\qquad\quad \left. - k^r_{\mathrm{HS_R}} \left(\theta^r_{\mathrm{diff}} - \theta^r_{w_R} \right) - \beta^r_{\mathrm{HS_R}} \left(\dot{\theta}^r_{\mathrm{diff}} - \dot{\theta}^r_{w_R} \right) \right\}
\end{cases}
\tag{3}
$$

where

$$
\begin{aligned}
J^r_{\mathrm{eq}_{dis}} = {} & J^r_{\mathrm{diff}} + 0.5 \left(J^r_{\mathrm{HS_R}} + J^r_{\mathrm{HS_L}} \right) \\
& + \left(J^r_{\mathrm{SS}} + \eta^r_{g1} J^r_{g1} i^r_{g1}{}^2 + \eta^r_{g2} J^r_{g2} i^r_{g2}{}^2 \right) i^r_{\mathrm{diff}}{}^2.
\end{aligned}
\tag{4}
$$

C. Dog Clutch Position

The position of the dog clutch assembly (controlled by the DC motor shown in Fig. 3) is modeled through a pure time delay τ^r_d and a first-order transfer function with time constant τ^r_{act}:

$$
\frac{x^r_{\mathrm{act}}}{x^r_{\mathrm{desired}}}(s) = \frac{e^{-\tau^r_d s}}{1 + \tau^r_{\mathrm{act}} s}.
\tag{5}
$$

The parameters in (5) were identified through specific experiments on the gearshift actuator.

IV. GEARSHIFT CONTROL WITH TORQUE-FILL

Gearshift control with torque-fill is an essential feature for the implementation of an advanced EMS, based on the selec-
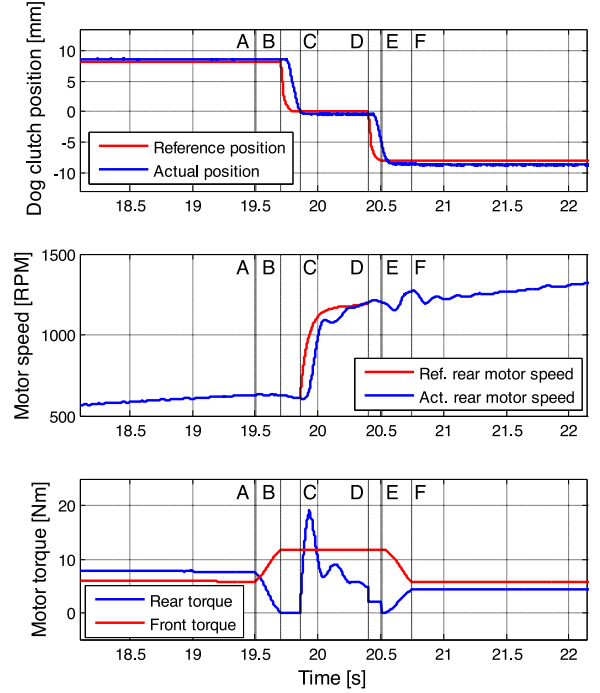

Fig. 6. Experimental downshift from second to first gear on the rear axle: dynamics of the gear actuator position, EM speed, and torques, with reference and actual values.

tion of the optimal state. This section describes the gearshift controller adopted for the experimental analysis of Section VI. To highlight its capability, experimental test results with the case study vehicle demonstrator are presented. The maneuver is a low-acceleration power-on downshift (from second to first gear) on the rear axle, while the front drivetrain remains in fixed first gear. Constant APP and front-to-total wheel torque distribution among the two axles (i.e., the reference torque distribution from the EMS, calculated for the current reference state) were imposed during the test. To demonstrate the possibility of uninterrupted vehicle acceleration during gearshifts, the values of the front and rear motor torques were set to be considerably lower than the maximum achievable values at that vehicle speed.

The downshift is split into five functional phases, indicated by the capital letters in Fig. 6, which shows the time histories of the dog clutch position, the reference and actual speeds of the rear motor, and the front and rear motor torque demands during the maneuver. The five phases are the following:

A-B: torque reduction phase;
B-C: displacement of the dog clutch from the initial gear (i.e., the second gear in this case) position to the neutral position;
C-D: inertia phase;
D-E: displacement of the dog clutch from the neutral position to the incoming gear (i.e., the first gear in this case) position;
E-F: torque increase phase.

During normal vehicle operation, the reference state and wheel torque distribution (hence the motor torque distribution as well) are set by the EMS (described in Section V) according to energy efficiency and drivability criteria. During gearshifts,

the transmission control unit (TCU) modifies the motor torque demands provided by the EMS.

The gearshift controller initially performs a motor torque reduction on the rear drivetrain (i.e., the motor torque reduction between points A and B in Fig. 6), while the front motor torque is increased to maintain an approximately constant vehicle traction force.

During the torque-fill process, the front EM torque demand is given by

$$T_{\mathrm{EM_{TF}}}^f = \frac{1}{i_{\mathrm{diff}}^f i_{g1}^f} \left(T_{\mathrm{EM_{EMS,g1}}}^f i_{\mathrm{diff}}^f i_{g1}^f + T_{\mathrm{EM_{EMS,g1}}}^r i_{g1}^r i_{\mathrm{diff}}^r \right.$$
$$\left. - \ T_{\mathrm{EM_{TCU}}}^r i_{\mathrm{diff}}^r i_{\mathrm{sel}}^r \right). \tag{6}$$

$T_{\mathrm{EM_{EMS,g1}}}^f$ is the torque demand for the front EM provided by the EMS, i.e., the torque the front motor would generate if the rear axle were not involved in the gearshift. $T_{\mathrm{EM_{EMS,g1}}}^r$ is the torque demand for the rear EM that would be output by the EMS if the rear drivetrain were already in first gear, i.e., the expected rear motor torque at the end of the gearshift. $T_{\mathrm{EM_{TCU}}}^r$ is the rear EM torque actually provided by the TCU during the gearshift (in reality, this is easily estimated starting from the rear motor torque demand and measured motor current). In this way, the overall wheel torque during the gearshift is virtually the same as the one expected at the completion of the gearshift, provided that the front EM has sufficient torque reserve to generate the torque demand given by (6). If the driver (or an automated driving system in the case of autonomous/semiautonomous driving) modifies the APP value during the maneuver, the EMS modifies the values of $T_{\mathrm{EM_{EMS,g1}}}^{f/r}$ accordingly, as they are functions of APP. During the inertia phase, when no gear is engaged on the rear axle, i_{sel}^r in (6) is set to 0, so that the total wheel torque is provided by the front electric drivetrain. A similar formulation of the reference torque is used for torque-fill during upshifts, or for the case of second gear operation of the axle not involved in the gearshift. Equation (6) neglects the effects of transmission efficiency and drivetrain inertia. This significantly simplifies the control system implementation, without any major drawback.

After the completion of the front motor torque reduction phase, the reference signal of the rear dog clutch position is varied from +9 mm (engaged second gear) to 0 mm (disengaged gear, phase B-C in Fig. 6). Once the dog clutch is disengaged, the inertia phase starts. In this phase, the EM speed has to be increased from the value corresponding to the second gear ratio to the level corresponding to the first gear ratio. To keep the computational demand low, a proportional-integral controller with antiwind-up was implemented to control the speed of the EM, i.e., to output the reference motor torque to track the desired motor speed profile. The gains of the controller were calculated using conventional methods in the frequency domain, i.e., gain and phase margins on the open-loop transfer function, and tracking bandwidth on the closed-loop transfer function. The control gains change through a look-up table, according to the selected driving mode and vehicle speed (which determines the duration of the inertia phase).
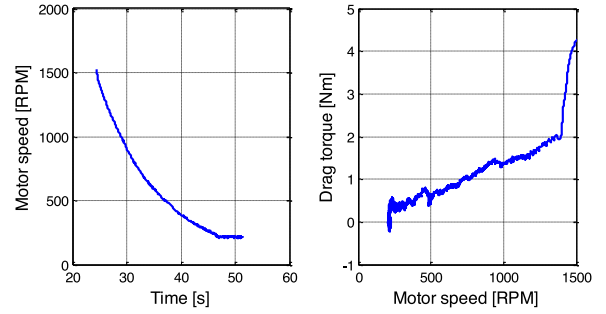

Fig. 7. Neutral gear test: motor speed reduction as a function of time (left) and drag torque as a function of motor speed (right).

During the inertia phase, the reference speed profile ("Ref. rear motor speed" in the second subplot of Fig. 6) is given by

$$\dot{\theta}_{\mathrm{EM_{desired}}}^r = \dot{\theta}_w^r \ i_{\mathrm{diff}}^r \ i_{g2}^r \ y\left(t_{\mathrm{IP}}\right). \tag{7}$$

The mean value of the two speed sensor signals on the rear wheels, $\dot{\theta}_w^r$, is used to calculate the reference speed of the rear EM. To reduce noise, the speed signals are filtered with a low-pass filter characterized by a time constant, τ_{filt}. The nondimensional factor $y(t_{\mathrm{IP}})$ is a normalization parameter defining the reference speed profile, so that it converges smoothly to the value for the new gear. t_{IP} is the output of a counter, which is activated by the TCU at the beginning of the inertia phase. The initial value of y is 1, so that (7) provides an initial value of the reference motor speed approximately equal to the actual motor speed at the beginning of the inertia phase. The final value of y is i_{g1}^r/i_{g2}^r for the downshift (i_{g2}^r/i_{g1}^r for an upshift), so that the final value of the reference motor speed is equal to that required for synchronization.

When the difference between the actual motor speed and the reference motor speed in the new gear is within a threshold (e.g., 10 RPM) for a sufficient amount of time (e.g., 200 ms), the reference signal to the dog clutch is set to the first gear value (point D in Fig. 6). In this phase, the TCU requests a sufficient amount of rear motor torque to overcome the friction losses within the drivetrain components rotating with the transmission's primary shaft. This avoids the beating of the dog clutch on the gear, which would extend the duration of the gearshift and introduce additional vibrations. Fig. 7 (left) plots the experimental time history of motor speed for a neutral gear condition of the drivetrain and zero torque demand, with the vehicle in standstill condition. By using the known values of the mass moments of inertia of the different components, it is possible to express the drag torque as a function of speed (right graph of Fig. 7). This characteristic can be input into a look-up table, which provides the level of rear motor torque demand during the phase D-E of Fig. 6.

Once the actuator has reached the final reference position, the second gear is considered to be engaged (point E in Fig. 6), and the rear motor torque demand is ramped up to the value specified by the EMS (point F in Fig. 6).

Even for gearshifts actuated in vehicle states using a single axle (states 5–8 in Fig. 4), it is possible to achieve torque-fill by momentarily using the inactive drivetrain to provide the

torque-filling action. This strategy implies a marginal actuation delay and energy consumption as the initially inactive motor has to be accelerated to the speed required for its synchronization, before the gearshift on the other drivetrain can be performed.

In general, the wheel torque increase on the drivetrain not involved in the gearshift could have an impact on the vehicle cornering response. In particular, at the cornering limit, the wheel torque variation can provoke an increase of vehicle understeer when the torque-filling action is performed by the front axle, and a reduction of understeer when the torque-filling action is actuated by the rear axle. However, as recently pointed out in [22], when the vehicle is far from its cornering limit, the increase of torque demand on the front axle could be the cause of a reduction (rather than an increase) of understeer. These effects are generally moderate for the case study vehicle, given the relatively limited wheel torque levels of the specific drivetrains. Moreover, wheel slip controllers (object of future publications), based on the reduction of the absolute value of the EM torque, are implemented on each axle of the vehicle demonstrator to prevent situations of significant wheel slip in traction or braking, which could happen during torque-fill, especially for low tire–road friction conditions.

V. ENERGY MANAGEMENT SYSTEM

The role of the EMS is to select the states and motor torque levels for each operating condition. The task must include consideration of vehicle drivability, e.g., an excessive number of state transitions should be prevented, despite the presence of the effective torque-fill controller described in Section IV. For actual industrial adoption, the EMS must be computationally efficient to run in real time and easily understandable and tuneable by vehicle engineers without specific experience in advanced control.

The EMS of this research is based on the results of an offline optimization, providing the look-up tables to be implemented online into the vehicle. The idea of the optimization is to select the state characterized by the lowest drivetrain power loss (i.e., with the highest efficiency), including the power loss contributions from the EMs, drives, and transmissions, for values of wheel torque demand and vehicle speed located on an assigned grid. If the optimal state is characterized by the front and rear axles both delivering/regenerating power (i.e., states 1–4; see Fig. 4), the optimization calculates the optimal wheel torque distribution as well.

Although this problem is much more complex than the control allocation algorithms for EVs with single-speed transmissions presented in the literature (see [14]–[16] and [23]–[25]), its number of variables is sufficiently small to be managed with an offline brute-force algorithm. In the brute-force approach, for a given wheel torque demand, vehicle speed, and (optionally) road grade, the evaluation of the cost function is carried out for all possible states and (for the states when both drivetrains are active) a grid of front-to-total wheel torque distributions. The method is independent from the properties of the power loss characteristics of the electric drivetrains, without the simplifying hypotheses (e.g., monotonically increasing power losses as
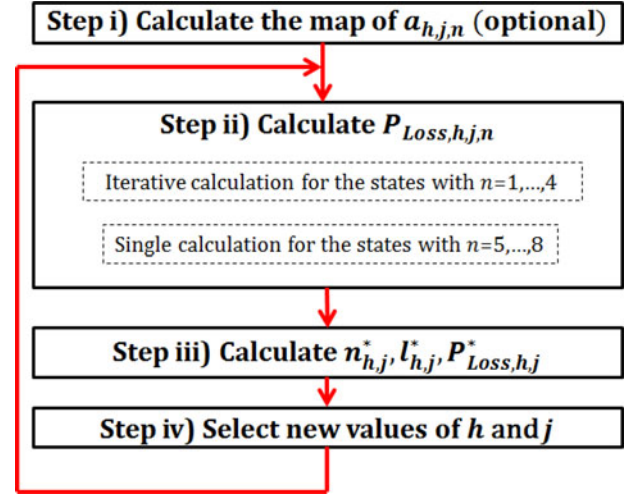

Fig. 8. Flowchart summarizing the main steps of the offline optimization for the EMS design.

functions of torque with a single inflexion point) and online computational complexity of the solutions from the literature. As a consequence, the effectiveness of the proposed algorithm is significant, provided that the grids of evaluation points used in the process include sufficient numbers of elements to generate solutions that are close to optimality.

In a first approximation, the offline algorithm consists of the following steps (see Fig. 8).

1) Definition of the grid of vehicle speeds, V_h, and total wheel torque demands, $T_{w,j}$, for which the optimization is run (at an assigned constant road grade). The individual points of the grid will be indicated as h and j in the remainder of the text. For each operating point, the corresponding longitudinal vehicle acceleration, $a_{h,j,n}$, is calculated, under the hypothesis of known mass and road gradient, through the following equation:

$$T_{w,j} - F_{\text{Aero}}(V_h) R_w - F_{\text{Roll}}(V_h) R_w - mgR_w \sin\alpha$$
$$= m_{\text{app},n} a_{h,j,n} R_w \qquad (8)$$

where the apparent vehicle mass, $m_{\text{app},n}$, function of the vehicle state, n, is

$$m_{\text{app},n} = m + 4\frac{J_w}{R_w^2} + \frac{J_{\text{eq}_{g1/g2/\text{dis}}}^f}{R_w^2} + \frac{J_{\text{eq}_{g1/g2/\text{dis}}}^r}{R_w^2}. \qquad (9)$$

With the approach discussed so far, the look-up tables resulting from the offline optimization receive inputs in terms of vehicle speed, wheel torque demand, and road gradient, when they are implemented on the vehicle. This formulation assumes that an inclinometer (or a road gradient estimator) and a mass estimator are present on the EV. An approximated option, available in the optimization, is to neglect the inertial effects, which simplifies the problem without significant drawbacks. This approach is useful especially if the vehicle is not equipped with an online estimator (or measurement system) of mass and road gradient, and if the inertial terms of the drivetrains

are negligible. In this simplified case, only the wheel torque demand and vehicle speed are required as inputs to the look-up tables for the online implementation of the controller.

2) For a selected operating point defined by h and j, the sum of the front and rear drivetrain power losses is evaluated for the possible states (see Fig. 4 and Table I). In particular:

a) For each of the feasible states with $1 \leq n \leq 4$, characterized by the action of both drivetrains, the power loss calculation has to be iterated for a set of front-to-total wheel torque distributions, equally spaced according to a grid (whose points are identified by the index l) defined during the process. To this purpose, at each iteration the torque on the front motor, $T_{\mathrm{EM},l}^f$, is imposed, and the rear motor torque, $T_{\mathrm{EM},h,j,n,l}^r$, is calculated with (10), to meet the equality constraint related to $T_{w,j}$, in addition to the inequality constraints (here omitted for conciseness) related to the drivetrain torque limitations.

$$T_{\mathrm{EM},h,j,n,l}^r = \frac{T_{w,j} - \eta_{g1/g2}^f i_{g1/g2}^f i_{\mathrm{diff}}^f T_{\mathrm{EM},l}^f}{\eta_{g1/g2}^r i_{g1/g2}^r i_{\mathrm{diff}}^r}$$

(10)

The resulting power loss for the operating condition defined by the indices h, j, n, and l is

$$P_{\mathrm{Loss},h,j,n,l} = P_{\mathrm{Loss,EM}+D}^f \left(T_{\mathrm{EM},l}^f, \; V_h, n \right)$$
$$+ \; P_{\mathrm{Loss,EM}+D}^r \left(T_{\mathrm{EM},h,j,n,l}^r, \; V_h, n \right)$$
$$+ \; P_{\mathrm{Loss},Tr}^f \left(T_{Tr,l}^f, \; V_h, n, a_{h,j,n} \right)$$
$$+ \; P_{\mathrm{Loss},Tr}^r \left(T_{Tr,j,l}^f, \; V_h, n, a_{h,j,n} \right)$$
$$+ \; P_{\mathrm{Roll}}^f \left(V_h, a_{h,j,n} \right) + P_{\mathrm{Roll}}^r \left(V_h, a_{h,j,n} \right). \quad (11)$$

$P_{\mathrm{Loss,EM}+D}^{f/r}$, $P_{\mathrm{Loss},Tr}^{f/r}$ and $P_{\mathrm{Roll}}^{f/r}$ are provided in the form of maps, partially used also in the simulation model in Section III. The previous torque balance equations [see (1) and (10)] included transmission efficiency values corresponding to the respective power losses (i.e., the efficiency and power loss maps must be consistent). The motor drive and transmission maps are typically functions of torque and angular speed; however, to accurately calculate the respective values, the values of n and $a_{h,j,n}$ are necessary as indicated in (11). The torque distribution with the minimum power loss for state n at the operating conditions defined by h and j is

$$\{l_{h,j,n}^*\} = \arg\min_l P_{\mathrm{Loss},h,j,n,l} . \quad (12)$$

The corresponding power loss is $P_{\mathrm{Loss},h,j,n}^*$.

b) For each feasible state with $5 \leq n \leq 8$, the minimum drivetrain power losses, $P_{\mathrm{Loss},h,j,n}^*$, are calculated using a single backward calculation, without the iterations of (11) and (12). In fact, the whole required traction or regenerative torque is delivered by one drivetrain, and the inactive drivetrain is only
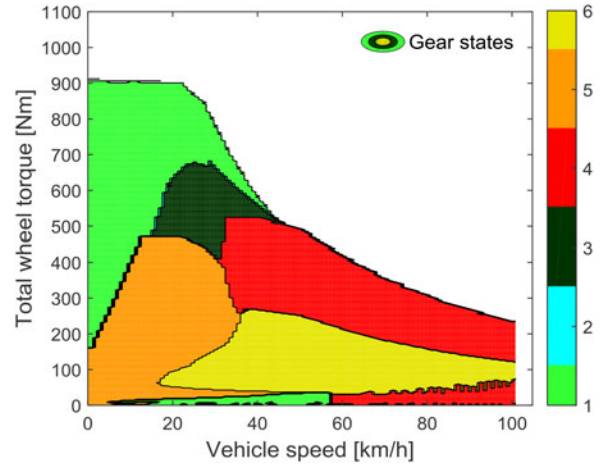

Fig. 9. Example of optimal gear state map for traction for the two-speed 4WD EV, according to the state numbering conventions in Fig. 4.

producing a rolling resistance torque, i.e., there is a single value of motor torque of the active drivetrain providing $T_{w,j}$ (single solution of the problem).

3) The state $n_{h,j}^*$, minimizing the drivetrain power losses at the operating condition defined by h and j, is calculated as

$$\{n_{h,j}^*\} = \arg\min_n P_{\mathrm{Loss},h,j,n}^*. \quad (13)$$

The corresponding front-to-total torque distribution and power loss are $l_{h,j}^*$ and $P_{\mathrm{Loss},h,j}^*$, respectively.

4) The result of (13) is stored in the memory. A new combination of h and j is selected and the procedure starts again from step 2 until all feasible combinations in the grid of V_h and $T_{w,j}$ (hj grid) are covered.

The whole procedure is repeated for multiple road grades in the case of EVs with appropriate measurement or state estimation of road grade and mass. Examples of optimization outputs are reported in Fig. 9 (optimal states) and Fig. 10 (optimal front-to-total wheel torque distributions) for traction conditions and 0% road grade. Fig. 9 suggests the selection of states with only one active axle (states 5 and 6) for low values of $T_{w,j}$, while for higher values of torque demand, both axles are active.

Apart from minor deviations, the optimal front-to-total wheel torque distributions in Fig. 10 mainly assume values of (or very close to) 0% and 50%. This means that for medium–high wheel torque demands, when both drivetrains are active with the same selected gear ratio, the most efficient solution for the case study vehicle consists of equally distributing the torque among the axles. These results are consistent with those recently presented in [23] for a simpler EV configuration with single-speed transmissions, without the problem of the optimal state selection.

The optimal states and torque distributions are compiled in the form of look-up tables for the online EMS implementation. The essential inputs of the look-up tables are the estimated vehicle speed and total wheel torque demand (from the drivability controller). Additional inputs (e.g., measured or estimated
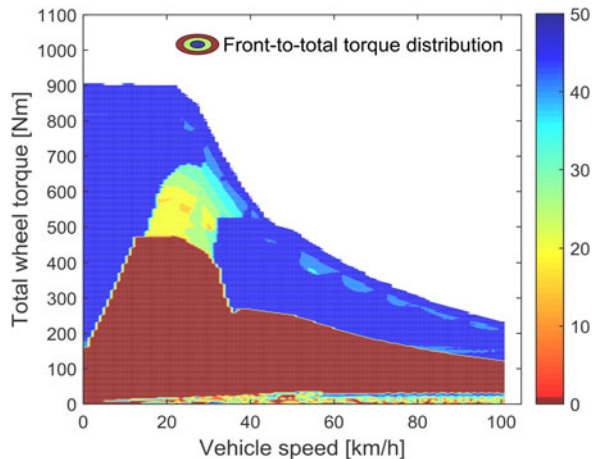
Fig. 10. Example of optimal torque distribution map for traction for the two-speed 4WD EV.

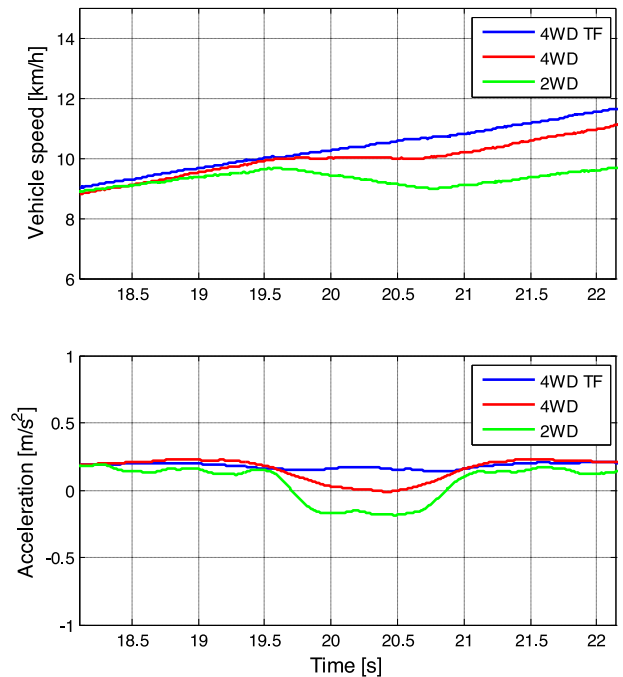| Signal	Discretization time [ms]	CAN bus	I/O
Rear motor speed $\dot\theta^r_{EM}$	20	Yes	I
Front motor speed $\dot\theta^f_{EM}$	20	Yes	I
Wheel speed $\dot\theta^r_w$	1	No	I
Dog clutch position x^r_{act}	1	No	I
Ref. dog clutch pos. $x^r_{desired}$	1	No	O
Rear motor torque T^r_{EM}	20	Yes	O
Front motor torque T^f_{EM}	20	Yes	O

Fig. 11. Example of vehicle speed and acceleration profiles during an experimental downshift maneuver with constant APP at 20%, for the 2WD and 4WD vehicles with and without torque-fill (TF).

road gradient, measured drivetrain temperatures) can be added depending on the specific application. The outputs are the reference states, and the front and rear torque demands.

As shown by the maps in Fig. 9 and 10, the offline optimization can produce look-up tables characterized by very small regions with a specific state, or very variable front-to-total wheel torque distributions. Frequent state transitions and wheel torque variations have a negative impact on vehicle drivability, despite the torque-fill capability of the drivetrain. Therefore, during the look-up table preparation process, a simplification of the maps can be performed, by deleting transitions toward states with small operating regions, and by increasing the smoothness of the front-to-total torque distribution. For the same reason, hysteresis in the management of the state transition phases needs to be implemented.

The resulting wheel torque demands are then modified by the TCU for gearshift management, and the active vibration controller (see the description in [26]) for reducing the torsional dynamics of the drivetrains and the subsequent vehicle acceleration oscillations. When required according to the estimated wheel slip conditions, the wheel torque demands are modified by the wheel slip controllers as well.

VI. RESULTS

A. Experimental Results with the Gearshift Controller

The gearshift strategy (see Section IV) was implemented on a dSPACE MicroAutoBox system installed on the case study EV. The main inputs and outputs of the controller are reported in Table II, together with the indication of their discretization time, and whether the controller area network (CAN) bus of the vehicle was used for the transmission of the respective signals (CAN buses cause time-variant delays and potential decay of the control system performance).

Fig. 11 shows an example of the experimentally measured speed and acceleration during a downshift on the rear axle, for the following cases.

1) The EV demonstrator used as a four-wheel-drive vehicle with torque-fill control ("4WD TF" in Fig. 11), i.e., involved in a transition from state 3 to state 1 (see the definition of the states in the legend of Fig. 4).

2) The EV demonstrator used as a four-wheel-drive vehicle without torque-fill control ("4WD" in Fig. 11), involved in the same state transition as in 1). The absence of torque-fill means that the front EM torque is not varied in order to limit the torque disruption induced by the shift on the rear axle, i.e., the front motor torque demand is equal to $T^f_{EM_{EMS,g1}}$ during the shift.

3) The EV demonstrator controlled as a rear-wheel-drive vehicle ("2WD" in Fig. 11), i.e., involved in a transition from state 6 to state 5.

For the test, the vehicle was accelerated from standstill with a fixed APP of 20%, i.e., ensuring the same overall wheel torque demand for cases 1–3. The gearshifts were initiated on the rear
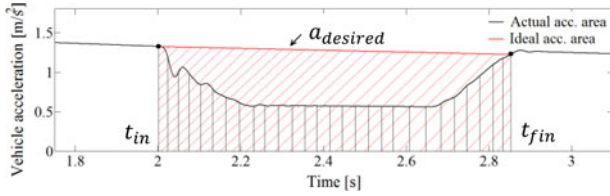
Fig. 12. Areas described by the longitudinal vehicle acceleration profiles during a gearshift.

TABLE III
EXPERIMENTAL VALUES OF THE GEARSHIFT PERFORMANCE INDICATORS

	2WD	4WD	4WD TF
PTPA [m/s²]	0.44	0.33	0.15
AR [-]	−0.92	0.35	1.17
IAE [m/s]	1.33	1.13	0.03

axle once a vehicle speed of ∼10 km/h was reached. The speed and acceleration profiles in Fig. 11 indicate a substantially seamless actuation of the gearshift with the torque-fill controller. On the other hand, the vehicle configurations without torque-fill control reach either approximately zero (see the "4WD" profile) or negative (see the "2WD" profile) values of longitudinal acceleration during the gearshift, because of the torque gap on the rear axle.

To objectively assess the gearshift quality, three performance indicators are adopted:
1) the peak-to-peak acceleration (PTPA);
2) the so-called area ratio (AR);
3) the integral of the acceleration error (IAE).

Specifically, PTPA is the difference between the maximum and minimum longitudinal acceleration values during the gearshift. This difference should be as low as possible, ideally zero in a seamless state transition. The indicators AR and IAE are functions of the deviation between the actual (a) and the ideal (a_desired) longitudinal accelerations during the gearshift. In particular, Fig. 12 shows the respective qualitative profiles and areas in the time domain.

In formulas

$$\mathrm{AR} = \frac{\text{Actual Area}}{\text{Ideal Area}} = \frac{\int_{t_\mathrm{in}}^{t_\mathrm{fin}} a\, dt}{[a(t_\mathrm{fin}) + a(t_\mathrm{in})](t_\mathrm{fin} - t_\mathrm{in})/2} \tag{14}$$

$$\mathrm{IAE} = \int_{t_\mathrm{in}}^{t_\mathrm{fin}} |a_\mathrm{desired} - a|\, dt. \tag{15}$$

From (14) and (15), good gearshift performance is achieved when AR is close to 1, and IAE is close to zero.

To check consistency and repeatability, each test was executed three times, and Table III reports the average values of the gearshift performance indicators. The experimental results confirm the significant gearshift quality improvement provided by the "4WD TF" vehicle, with respect to the vehicle setups without the torque-fill controller. For example, the PTPA is only 0.15 m/s² for the "4WD TF," against the 0.33 and
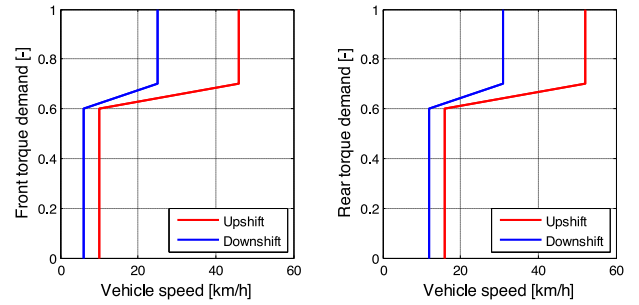

Fig. 13. Front and rear gearshift maps.

TABLE IV
ENERGY CONSUMPTION AT CONSTANT SPEED

Vehicle speed [km/h]	Baseline controller [Wh/km]	Optimized controller [Wh/km]	Reduction [%]
30	38.80	37.31	−3.84
50	53.03	51.02	−3.79
70	74.64	68.53	−8.19

0.44 m/s² for the "4WD" and "2WD" cases, respectively. Also, the "4WD TF" vehicle provides values of AR and IAE very close to the optimal ones, and according to the subjective feedback of the test driver and the passengers, the performed gearshifts could not be actually perceived by the vehicle occupants.

B. Simulation Results with the EMS

To examine the benefits of the optimization-based EMS, the forward facing vehicle simulation model discussed in Section III was used for the assessment of the energy consumption in the following driving conditions:
1) vehicle operation on a road with zero longitudinal gradient at the constant speeds of 30, 50, and 70 km/h;
2) vehicle operation along the urban part of the New European Driving Cycle, i.e., the so-called Urban Driving Cycle (UDC), and the J10-15 cycle.

The analysis compares the energy efficiency performance of a conventional controller, here defined as baseline controller, and the EMS controller implemented according to the description in Section V. In particular, the baseline controller imposes a constant front-to-total wheel torque distribution equal to 50% (i.e., both drivetrains are always active), and a state selection through gearshift maps, similar to those of conventional vehicles with automated transmissions. These are functions of the torque demand on each axle (i.e., the ratio between the actual and the maximum achievable wheel torque, which depends on the actual motor speed) and vehicle speed, as shown in Fig. 13. The offset between the front and rear axle maps in Fig. 13 is imposed in order to achieve a single gearshift at a time, without provoking a simultaneous torque interruption on the two drivetrains. A driver model, based on the combination of feedforward and feedback control, was used for tracking the reference speed profiles.

The constant speed results in Table IV suggest that the optimized controller brings energy savings of up 8.2% (at

TABLE V
ENERGY CONSUMPTION DURING THE UDC AND J10-15 DRIVING CYCLES

Driving Cycle	Baseline controller [Wh]	Optimized controller [Wh]	Reduction [%]
UDC	226.4	221.0	–2.38
J10-15	405.2	381.5	–5.84

70 km/h) by appropriate selection of the gear state and front-to-total torque distribution. Table V shows the results of the two controllers along the UDC and the J10-15 cycle, with reductions in the energy consumption for the optimization-based controller of ∼2.4% and ∼5.8%, respectively. It is evident that the complexity of the optimized controller is justified by the magnitude of the energy savings for the specific vehicle and drivetrain dataset. In particular, it was observed that a significant part of the driving cycles with the optimized EMS is ran in single-axle states, while the second axle is in neutral gear. The single-axle states are selected especially in conditions of medium-low torque demands.

VII. CONCLUSION

This paper presented a gearshift strategy with torque-fill capability and an EMS for a 4WD vehicle equipped with two electric drivetrains, including two-speed transmissions. The analysis allows the following conclusions.

1) The appropriate control of both electric drivetrains significantly reduces the torque gap during gearshifts. This allows using two-speed transmission systems characterized by significant mechanical simplicity, i.e., not requiring the adoption of friction clutches with the respective actuators.

2) The gearshift controller with torque-fill was implemented on an EV demonstrator and experimentally assessed with respect to the performance of other two more conventional gearshift methodologies. Three gearshift performance indicators (PTPA, AR, and IAE) consistently showed the significant performance improvement caused by the torque-fill controller, in terms of quality of the measured longitudinal acceleration profile, which is substantially coincident with the reference profile for gearshifts at medium-low torque demands.

3) A computationally efficient EMS for the selection of the optimal state and front-to-total wheel torque distribution was presented. The control outputs are based on multi-dimensional look-up tables, obtained through an offline optimization procedure, considering the efficiency maps of the electric drivetrain components. The optimization shows that at medium-low torque demands, it is convenient to use a single electric drivetrain, while the second drivetrain is kept in neutral gear. At high torque demands, when the front and rear drivetrains operate in the same gear, the optimal solution is represented by a front-to-total torque distribution close to 50%.

4) The simulation results indicate that with the specific vehicle dataset, the optimized EMS, compared to a more conventional baseline controller, brings energy consump-

tion reductions of up to 8.2% and 5.8%, respectively, at constant speed and along driving cycles.

REFERENCES

[1] J. Miller, *Propulsion Systems for Hybrid Vehicles* (*IET Power and Energy Series*), vol. 45. Stevenage, U.K.: IET, 2004.

[2] [Online]. Available: http://www.teslamotors.com/en_GB/roadster/technology. Accessed on: Aug. 10, 2015.

[3] T. Holdstock, A. Sorniotti, M. Everitt, M. Fracchia *et al.*, "Energy consumption analysis of a novel four-speed dual motor drivetrain for electric vehicles," in *Proc. IEEE Veh. Power Propul. Conf.*, 2012, pp. 295–300.

[4] U. Knödel, "Electric axle drives for axle split hybrids and EV applications," in *Proc. 9th Eur. All-Wheel Drive Congr.*, 2009.

[5] S. Riderknecht and T. Meier, "Electric power train configurations and their transmission systems," in *Proc. Int. Symp. Power Electron., Elect. Drives, Autom. Motion*, 2010, pp. 1564–1568.

[6] A. Sorniotti *et al.*, "Analysis and simulation of the gearshift methodology for a novel two-speed transmission system for electric powertrains with a central motor," *IMechE Part D: J. Automobile Eng.*, vol. 226, no. 7, pp. 915–929, 2012.

[7] S. De Pinto, P. Camocardi, A. Sorniotti, G. Mantriota, P. Perlo, and F. Viotto, "A four-wheel-drive fully electric vehicle layout with two-speed transmissions," in *Proc. IEEE Veh. Power Propul. Conf.*, 2014, pp. 1–6.

[8] D. Paul, "Multi-speed transmissions for electric vehicle applications," in *Proc. U.K. Low Carbon Veh. Event*, 2011.

[9] M. Müller, "Manual transmission of a motor vehicle," U.S. Patent 5 363 712, 1994.

[10] X. Zhou, P. Walker, and N. Zhang, "Performance improvement of a two speed EV through combined gear ratio and shift schedule optimization," *SAE Tech.* Paper 2013-01-0477, 2013.

[11] C. Yin, F. Zhu, J. Shu, and M. Zhang, "Two-speed transmission and electric vehicle," U.S. Patent 2015/0 141 191A1, 2015.

[12] S. T. Razzacki, "Design methodology for a compact dual clutch transmission (DCT)," *SAE Tech.* Paper 2009-01-0511, 2009.

[13] F. Bottiglione, S. De Pinto, and G. Mantriota, "Infinitely variable transmissions in neutral gear: Torque ratio and power re-circulation," *Mech. Mach. Theory*, vol. 74, no. 3, pp. 285–298, 2014.

[14] Y. Chen and J. Wang, "Fast and global optimal energy-efficient control allocation with applications to over-actuated electric ground vehicles," *IEEE Trans. Control Syst. Technol.*, vol. 20, no. 5, pp. 1202–1211, Sep. 2012.

[15] Y. Chen and J. Wang, "Design and experimental evaluations on energy efficient control allocation methods for overactuated electric vehicles: Longitudinal motion case," *IEEE/ASME Trans. Mechatronics*, vol. 19, no. 2, pp. 538–548, Apr. 2014.

[16] Y. Chen and J. Wang, "Energy-efficient control allocation with applications on planar motion control of electric ground vehicles," in *Proc. Amer. Control Conf.*, 2011, pp. 2719–2724.

[17] [Online]. Available: http://www.moby-ev.eu. Accessed on: Aug. 10, 2015.

[18] S. De Pinto, A. Sorniotti, P. Gruber, P. Camocardi, P. Perlo, and F. Viotto, "Gearshift control with torque-fill for a 4-wheel-drive fully electric vehicle," in *Proc. Int. Conf. Sustain. Mobility Appl., Renewables Technol.*, 2015, pp. 1–6.

[19] [Online]. Available: http://www.oerlikon.com/graziano/en/products/automotive/transfer-cases-for-full-electric-zero-emission-vehicles-2. Accessed on: Aug. 10, 2015.

[20] H. Pacejka, *Tyre and Vehicle Dynamics*, 2nd ed. Oxford, U.K.: Butterworth-Heinemann, 2005.

[21] E. Galvagno, D. Morina, A. Sorniotti, and M. Velardocchia, "Drivability analysis of through-the-road-parallel hybrid vehicles," *Meccanica*, vol. 48, no. 2, pp. 351–366, 2013.

[22] F. Bucchi and F. Frendo, "A new formulation of the understeer coefficient to relate yaw torque and vehicle handling," *Veh. Syst. Dyn.*, vol. 54, no. 6, pp. 831–847, 2016.

[23] A. M. Dizqah, B. Lenzo, A. Sorniotti, P. Gruber, S. Fallah, and J. De Smet, "A fast and parametric torque distribution strategy for four-wheel-drive energy efficient electric vehicles," *IEEE Trans. Ind. Electron.*, vol. 63, no. 7, pp. 4367–4376, Jul. 2016.

[24] H. Fujimoto and S. Harada, "Model-based range extension control system for electric vehicles with front and rear driving-braking force distributions," *IEEE Trans. Ind. Electron.*, vol. 62, no. 5, pp. 3245–3254, May 2015.

[25] X. Yuan and J. Wang, "Torque distribution strategy for a front- and rear-wheel-driven electric vehicle," *IEEE Trans. Veh. Technol.*, vol. 61, no. 8, pp. 3365–3374, Oct. 2012.

[26] L. De Novellis *et al.*, "Direct yaw moment control actuated through electric drivetrains and friction brakes: Theoretical design and experimental assessment," *Mechatronics*, vol. 26, pp. 1–15, 2015.

Stefano De Pinto received the M.Sc. degree in mechanical engineering and the Ph.D. degree in mechanical and automotive engineering from the Politecnico di Bari, Bari, Italy, in 2011 and 2015, respectively.

He was a Research Fellow in advanced vehicle engineering with the University of Surrey, Guildford, U.K. He is a Technical Specialist with McLaren Automotive Ltd., Woking, U.K. His main research interests include hybrid electric vehicles, electric vehicles, and vehicle dynamics.

Pablo Camocardi received the B.Sc. and Ph.D. degrees in electrical engineering from the National University of La Plata, La Plata, Argentina, in 2003 and 2011, respectively.

He was a Research Fellow in advanced vehicle engineering with the University of Surrey, Guildford, U.K. He is a Senior Researcher with Brose Fahrzeugteile GmBH, Würzburg, Germany. His research interests include research and development, control and modeling, electric vehicles, electric machines, and renewable energy.

Aldo Sorniotti (M'12) received the M.Sc. degree in mechanical engineering and the Ph.D. degree in applied mechanics from the Politecnico di Torino, Turin, Italy, in 2001 and 2005, respectively.

He is a Reader in advanced vehicle engineering and the coordinator of the Automotive Engineering Research Group with the University of Surrey, Guildford, U.K. His research interests include vehicle dynamics control and transmissions for electric and hybrid vehicles.

Patrick Gruber received the M.Sc. degree in motorsport engineering and management from Cranfield University, Cranfield, U.K., in 2005, and the Ph.D. degree in mechanical engineering from the University of Surrey, Guildford, U.K., in 2009.

He is a Senior Lecturer in advanced vehicle systems engineering with the University of Surrey. His current research interests include tire dynamics and development of novel tire models.

Pietro Perlo received the M.Sc. degree in general physics from the University of Torino, Turin, Italy, in 1980.

He then continued the collaboration with the Institute of Physics of the University of Torino for 15 years as a Contract Professor for short courses on applied optics. In 1981 he joined Centro Ricerche Fiat, where he was a Senior Director until 2011. Since 2011, he has been the President and owner of Interactive Fully Electric Vehicles, Turin, and the President of P-GEVS, SMEs addressing the development of novel electric vehicles. He is a major contributor to the evolution of the European roadmap on electromobility and a member of the European Union H2020 Advisory Board for "Smart, Green and Integrated Transports."

Fabio Viotto received the M.Sc. degree in mechanical engineering from the Politecnico di Torino, Turin, Italy, in 1998.

He was with the Research and Development Department, Modulo UNO, where he worked on noise and vibration control. Since 2008, he has been a Project Engineer with Oerlikon Graziano SpA, Turin. His main research interests include the development of novel transmission systems for electric and hybrid electric vehicles.